A FINITE ELEMENT METHOD FOR PREDICTION OF MACROSEGREGATION WITH SOLIDIFICATION COLUMNAR

Qipeng Chen, Houfa Shen*

Key Laboratory for Advanced Materials Processing Technology, Ministry of Education,
School of Materials Science and Engineering, Tsinghua University, Beijing 100084, China

Abstract

A finite element method (FEM) was developed to predict macrosegregation during alloys solidification with columnar structure. A fractional step method was employed to solve the thermosolutal convection in the mushy zone with a damping convection. The velocity and pressure were decoupled and interpolated by equal-order linear triangular elements. The time derivative terms were discretized by a fully implicit Euler backward method. The convection-diffusion equations of energy, solute and momentum were spatially discretized by the consistent SUPG method, and the terms of convection, diffusion, pressure gradient, Darcy drag, and buoyancy were integrated using the second-order Crank-Nicolson method. A solution procedure was designed to couple the resolutions of conservations of energy, solute and momentum, as well as the microsegregation model at an overall computational efficiency and accuracy. The FEM was applied to predict macrosegregation during solidification of Pb-18wt%Sn alloy in a rectangular mold. The macrosegregation maps, temperature fields, velocity fields and liquid fraction fields, as well as evolutions of liquid fraction, average mass concentration and velocity magnitude were presented.

Keywords: *finite element, macrosegregation, solidification, fractional step, equal-order element*

1. INTRODUCTION

Macrosegregation is a defect of chemical heterogeneities in many solidification processes, and it deteriorates microstructure and mechanical properties of the products. Macrosegregation is caused by relative movements of solid and liquid phases, which are related to the transport phenomena that take place over several characteristic length scales ([1] Lesoult 2005). Numerical models were originally concentrated on the effect of solute redistribution, and included only buoyancy-driven convection in the interdendritic liquid ([2] Flemings & Nereo 1967). Subsequently, transport equations accounting for different length scales were derived by a volume averaging technique ([3] Ni & Beckermann 1991) or mixture theory ([4] Bennon & Incropera 1987). After that, multiphase models ([5] Li et al. 2012) that couples multiple sets of conservation equations for different phases were developed. Nevertheless, the coupling of global multiphase transport phenomena with microscopic solidification kinetics is extremely complex and requires large amount of computation resources. As a consequence, the one-domain model based on the volume averaging technique or mixture theory is still fundamental and inevitable in practice.

The major advantage of finite element method (FEM) is the flexibility of mesh discretization, and arbitrarily shaped domains can be easily approximated by unstructured meshes with high accuracy. The disadvantage is that larger computation amount and higher memory are required than other numerical methods such as the finite volume method. In the case of solidification, the efficiency is lower further due to another range of factors. Firstly, a coupled system of equations resulting from conservations of energy, mass, momentum and solute must be solved. Nonlinearities in these equations should be dealt with carefully, and a specific solution procedure is needed to couple different transport phenomena efficiently. Secondly, the numerical solution of incompressible flows is inherent difficult, because the velocity and pressure are coupled by the incompressibility constraint implicitly.

The objective of the present work is to present a finite element formulation for the prediction of macrosegregation with solidification columnar ([6] Bellet et al. 2009). A fractional step method ([7] Choi, Choi & Yoo 1997), which was originally used in Navier-Stokes equations, was extended to solve

the thermosolutal convection during solidification. The formulation was applied to a reference case. The results and comparison with those obtained by the FEM code of CEMEF ([8] Combeau et al. 2011, [9] Combeau et al. 2012) were presented.

2. METHODS

2.1. Mathematical model

The "minimal" model proposed by Bellet et al. (2009) for solidification of binary alloys was implemented in present work. The liquid flow is assumed as laminar and Newtonian, the solid phase is fixed and non-deformable, and the mushy zone is treated as a porous medium with isotropic permeability defined by the Carman-Kozeny relation ([10] Carman 1937). Local thermodynamic equilibrium is kept at the solid/liquid interface, with perfect solute diffusion in both phases (lever rule). All properties in both solid and liquid phases are equal and constant, except the density in the buoyancy term, which is determined by the Boussinesq approximation. The conservation equations of mass, momentum, energy and solute are written as follows:

Total mass Conservation:

$$\nabla \cdot \mathbf{V} = 0 \tag{1}$$

where $\boldsymbol{V}$ is the average liquid velocity vector.

Momentum Conservation for liquid phase:

$$\rho \frac{\partial \mathbf{V}}{\partial t} + \frac{\rho}{g_l}(\nabla \mathbf{V})\mathbf{V} = \nabla \cdot (\mu_l \nabla \mathbf{V}) - g_l \nabla p - \frac{\mu_l}{K} g_l \mathbf{V} + g_l \rho_b \boldsymbol{g} \tag{2}$$

where p is the pressure, t the time, ρ the reference density, ρ_b the density in the buoyancy term, g_l the liquid fraction, μ_l the dynamic viscosity of the liquid, K the permeability in the mushy zone, and $\boldsymbol{g}$ the gravity vector.

Energy Conservation:

$$\rho \frac{\partial H}{\partial t} + \rho c_p \nabla T \cdot \mathbf{V} - \nabla \cdot (\lambda \nabla T) = 0 \tag{3}$$

where H is the volume averaged specific enthalpy, T the temperature, λ the average thermal conductivity, and c_p the specific heat.

Solute Conservation:

$$\frac{\partial w}{\partial t} + \nabla w_l \cdot \mathbf{V} = 0 \tag{4}$$

where w and w_l are the average mass concentration and the average mass concentration in liquid, respectively.

The supplementary relations are given by:

Permeability of the mushy zone:

$$K = \frac{\lambda_2^{\,2}}{180} \frac{g_l^{\,3}}{(1 - g_l)^2} \tag{5}$$

where λ_2 is the secondary dendrite arm spacing.

Density in the buoyancy term:

$$\rho_b = \rho\left[1-\beta_T\left(T-T_{ref}\right)-\beta_w\left(w_l-w_{ref}\right)\right] \tag{6}$$

where β_T is the thermal expansion coefficient, β_w the solutal expansion coefficient, T_{ref} the reference temperature, and w_{ref} the reference mass concentration.

Volume averaged enthalpy:

$$H = c_p T + g_l L \tag{7}$$

where L is the latent heat of fusion.

Microsegregation model (lever rule):

$$w_s = k_p w_l \tag{8}$$

$$w = g_l w_l + g_s w_s \tag{9}$$

$$g_l + g_s = 1 \tag{10}$$

$$T = T_m + m_l w_l \tag{11}$$

where w_s is the average mass concentration in solid, k_p the partition coefficient (<1), g_s the solid fraction, T_m the melt temperature of pure solvent, and m_l the liquidus slope (<0).

2.2. Fractional step method

In order to circumvent the difficulty of solving a large system induced by mixed finite element methods, a fully implicit four-step fractional method ([7] Choi, Choi & Yoo 1997) originally used to solve the Navier-Stokes equations was extended to solve the thermosolutal convection which has a damping in the mushy zone during solidification. Using this method, the coupled system of conservation equations of mass and momentum was split into several decoupled systems of much smaller size, which can be solved easily with much less computational cost. The time derivative was discretized by a fully implicit Euler backward method. The terms of convection, diffusion, pressure gradient, Darcy drag, and buoyancy were integrated using the Crank-Nicolson method which has second-order accuracy. The resulting time-discrete equations of the decoupled systems corresponding to Eq.(1-2) are written as follows:

$$\frac{\rho}{g_l}\frac{\hat{\mathbf{V}}-\mathbf{V}^n}{\Delta t}+\frac{1}{2}\frac{\rho}{g_l^2}\left[\left(\nabla\hat{\mathbf{V}}\right)\hat{\mathbf{V}}+\left(\nabla\mathbf{V}^n\right)\mathbf{V}^n\right]=\frac{1}{2}\frac{\mu_l}{g_l}\left(\nabla^2\hat{\mathbf{V}}+\nabla^2\mathbf{V}^n\right)-\nabla p^n-\frac{1}{2}\frac{\mu_l}{K}\left(\hat{\mathbf{V}}+\mathbf{V}^n\right)+\rho_b\boldsymbol{g} \tag{12}$$

$$\frac{\rho}{g_l}\frac{\mathbf{V}^*-\hat{\mathbf{V}}}{\Delta t}=\frac{1}{2}\nabla p^n \tag{13}$$

$$\nabla^2 p^{n+1}=\frac{2\rho}{\Delta t}\nabla\cdot\mathbf{V}^* \tag{14}$$

$$\frac{\rho}{g_l}\frac{\mathbf{V}^{n+1}-\mathbf{V}^*}{\Delta t}=-\frac{1}{2}\nabla p^{n+1} \tag{15}$$

where superscript n denotes the time level, and Δt the time step. The liquid fraction g_l, permeability K and density ρ_b are all evaluated at time level n+1/2. As the permeability is highly nonlinear with the liquid fraction and unable to be integrated accurately, the Darcy drag term was included only in Eq.(12) to improve the computational efficiency. With the pressure gradient term treated explicitly, an intermediate velocity $\hat{\mathbf{V}}$ was first solved by Eq.(12), and substituted to Eq.(13) to calculate another intermediate velocity $\mathbf{V}^*$. Then, the pressure was obtained by the pressure Poisson equation Eq.(14)

derived from the incompressibility constraint. Finally, the velocity was corrected by Eq.(15) with the new pressure.

To understand why the decoupled systems can approximate the original system, one can take the sum of Eqs.(12), (14), and (15), and get

$$\frac{\rho}{g_l}\frac{\mathbf{V}^{n+1}-\mathbf{V}^n}{\Delta t}+\frac{1}{2}\frac{\rho}{g_l^2}\left[\left(\nabla\hat{\mathbf{V}}\right)\hat{\mathbf{V}}+\left(\nabla\mathbf{V}^n\right)\mathbf{V}^n\right]=\frac{1}{2}\frac{\mu_l}{g_l}\left(\nabla^2\hat{\mathbf{V}}+\nabla^2\mathbf{V}^n\right)-\frac{1}{2}\left(\nabla p^{n+1}+\nabla p^n\right)-\frac{1}{2}\frac{\mu_l}{K}\left(\hat{\mathbf{V}}+\mathbf{V}^n\right)+\rho_b\boldsymbol{g} \tag{16}$$

Obviously, the approximation accuracy depends on the accuracy that $\hat{\mathbf{V}}$ approximates $\mathbf{V}^{n+1}$. On the other hand, according to Eqs.(13) and (15), the intermediate velocity can be expressed as follows:

$$\hat{\mathbf{V}}=\mathbf{V}^{n+1}+\frac{\Delta t}{2\rho}g_l\left(\nabla p^{n+1}-\nabla p^n\right)=\mathbf{V}^{n+1}+O\left(\Delta t^2\right) \tag{17}$$

This indicates that the decoupled systems is a good approximation to the original system. As the fully implicit time-stepping scheme is used, the time step is restricted only by the solution accuracy. Furthermore, it has been demonstrated that the four-step fractional method can well accommodate the lowest equal-order polynomial pairs (i.e., P1/P1 or Q1/Q1) ([7] Choi, Choi & Yoo 1997).

3. RESULTS AND DISCUSSION

As a response to the reference case proposed by Bellet et al. (2009) for macrosegregation during solidification of Pb-18wt%Sn alloy, results predicted by the present FEM code, and comparison with those obtained by the FEM code of CEMEF, i.e., the software R2SOL ([8] Combeau et al. 2011, [9] Combeau et al. 2012), are presented in this section. The configuration chosen is a 2D ingot casting which is schematically described in Fig. 1. A quiescent and homogeneous liquid binary metal at the liquidus temperature corresponding to the nominal mass concentration is initially contained in a rectangular mold with 60 mm height and 100 mm width. The mold is cooled down symmetrically on the left and right walls which are imposed a Fourier-type boundary condition, and insulated on the top and bottom walls. A no-slip condition for the velocity is imposed on all walls. Thus, assuming the symmetry of the solution, the calculation domain can be simplified as a half of the mold. In order to make results comparable with those obtained by the FEM code of CEMEF, a uniform structured mesh with 201×241 nodes (the average mesh size is 2.5×10^{-4} m) and a fixed time step of 5×10^{-3} s are used in the present simulations. More details of the configuration, and all thermophysical parameters can be referred to Bellet et al. (2009).

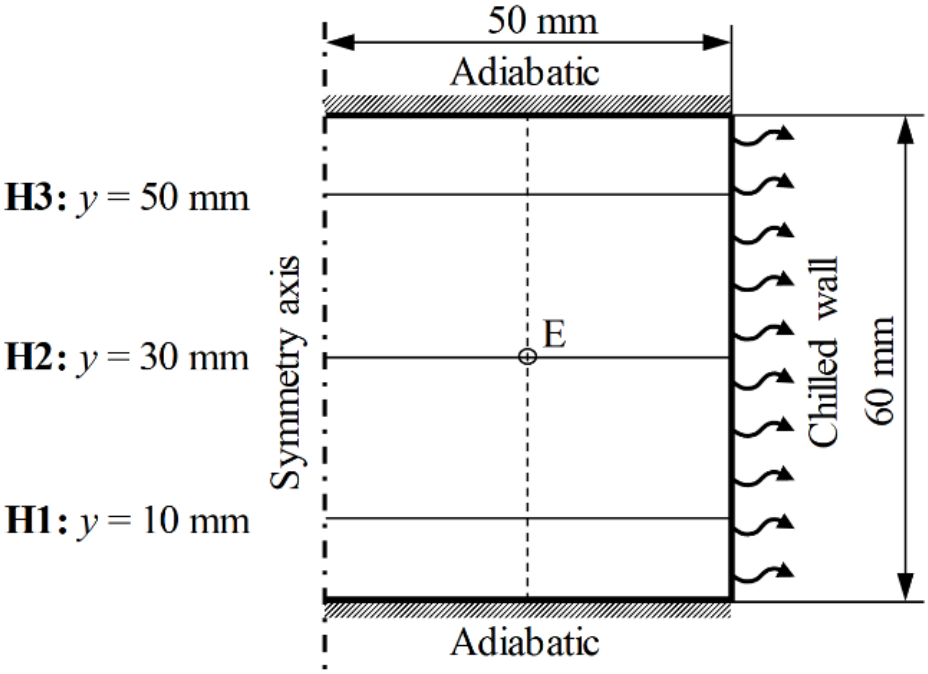

Fig. 1. Schematic of the solidification configuration of the two reference cases

The temperature field, velocity field and liquid fraction field, as well as the segregation maps at 120 s and the end of solidification of the Pb-18wt%Sn ingot are shown in Fig. 2. As the liquid density decreases with the decreasing temperature along the liquidus line, the circulation of the liquid resulting from the solidification in the ingot is counterclockwise, as shown in Fig. 2(b). Due to the higher damping for the flow, the isotherm is more vertical with lower liquid fraction, as shown in Fig. 2(a). In the upper left region where the liquid fraction is high, however, the isotherms bend to the left because of the counterclockwise circulation of the liquid. In Fig. 2(b), some channels, where the liquid fraction is locally greater, have already been formed. They originate from the early stage of solidification, indicating that the formation of channels is related to the flow at high liquid fraction. Because of smaller penetration resistance, these channels become preferential paths for the flow of the solute enriched liquid. In Fig. 2(c), there already are developed positive segregation inside these channels and severe negative segregation in the vicinity of them, respectively. Moreover, it can be seen from the final segregation map shown in Fig. 2(d) that the channels formed previously (Fig. 2(c)) are all retained and further developed. The final macrosegregation can be recognized as a positive segregation band along the axis of symmetry, a negative segregation pocket in the lower region, and the segregation channels inclined to the upper left in the upper right region. Compared to the final macrosegregation map obtained by the FEM code of CEMEF ([9] Combeau et al. 2012), general agreement can be observed, though differences can be found in detailed characteristics.

Evolutions of the liquid fraction and average mass concentration of Sn at point E (shown in Fig. 1) are shown in Fig. 3. Following the microsegregation model, the solute Sn is redistributed at the solid/liquid interface, leaving a Sn enriched liquid and a Sn depleted solid. As the Sn enriched liquid is brought from the mushy zone into the bulk liquid by the circulation of the liquid, the average mass concentration of Sn in the mushy zone decreases. It is notable that the average mass concentration of Sn decreases until the liquid fraction is less than 0.2, indicating that the interdendritic liquid flow in the mushy zone is responsible for macrosegregation. In the case of low liquid fraction, compared to the terms of pressure gradient, Darcy drag, and buoyancy in the momentum equation Eq.(2), the convective term in this equation is negligible.

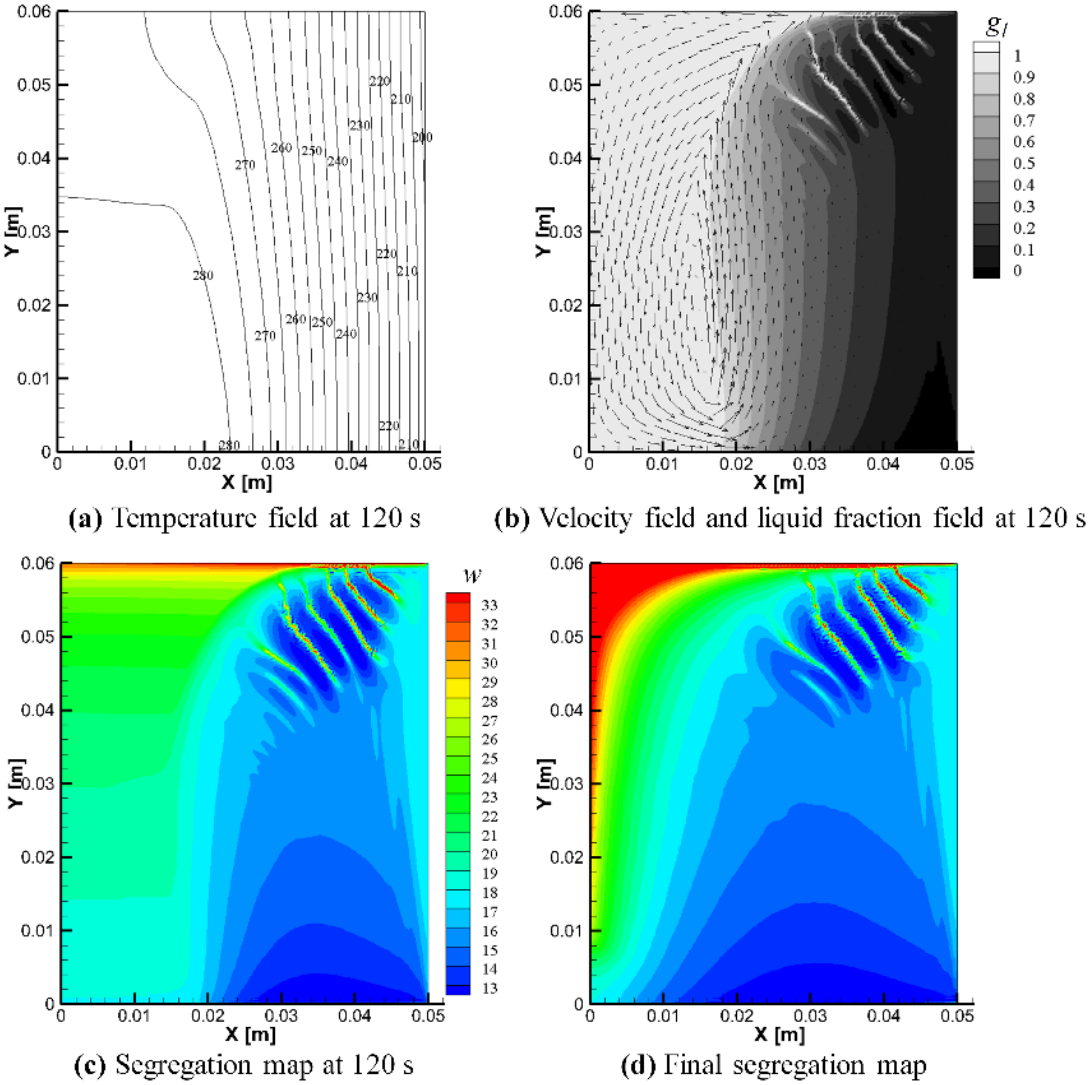

(a) Temperature field at 120 s **(b)** Velocity field and liquid fraction field at 120 s

(c) Segregation map at 120 s **(d)** Final segregation map

Fig. 2. Physical fields predicted during solidification of the Pb-18wt%Sn ingot

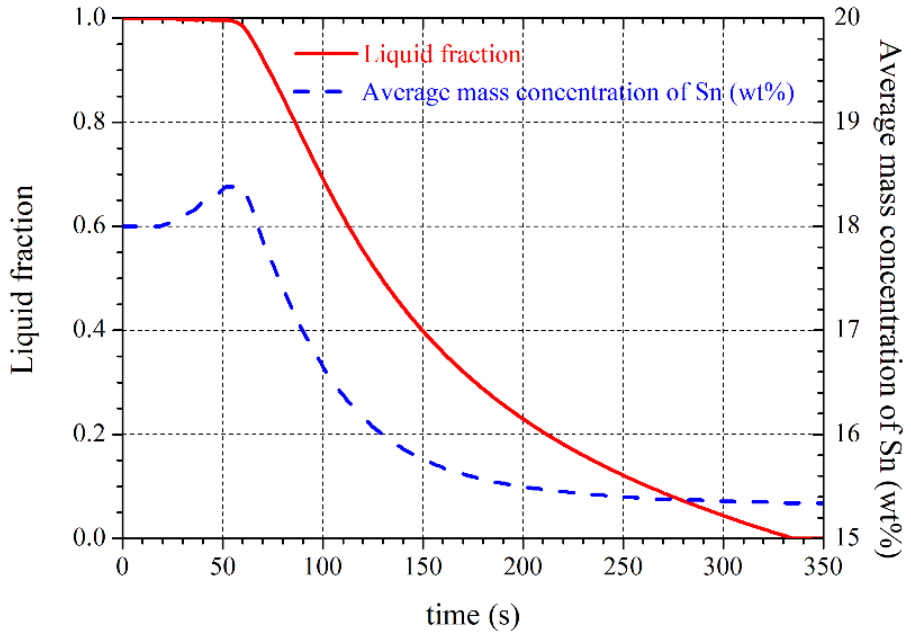

Fig. 3. Evolutions of the liquid fraction and average mass concentration of Sn at point E in the Pb-18wt%Sn ingot during solidification

4. CONCLUSIONS

A finite element formulation for the prediction of macrosegregation in columnar solidification alloys has been developed. In this formulation, a fractional step method, which was originally used in Navier-Stokes equations, was extended to solve the thermosolutal convection that has a damping in the mushy zone during solidification. By using this method, the velocity and pressure in the coupled system of conservations of mass and momentum were decoupled and interpolated by equal-order linear triangular elements, resulting in several systems of much smaller size, which can be solved easily with much less computational cost. For convection-diffusion equations of energy, solute and momentum, the consistent SUPG method and the second-order Crank-Nicolson scheme were used to the discretization and integration over the spatial domain, respectively. The resolutions of conservations of energy, solute and momentum, as well as the microsegregation model were coupled by a solution procedure at an overall computational efficiency and accuracy.

The finite element formulation was applied to the reference case proposed by Bellet et al. (2009). On one hand, macrosegregation maps, temperature fields, velocity fields, and liquid fraction fields, as well as evolutions of liquid fraction, average mass concentration, and velocity magnitude were obtained, showing a good capacity of the present finite element formulation for numerical simulation of macrosegregation. On the other hand, the macrosegregation patterns obtained by the present FEM code and the FEM code of CEMEF ([8] Combeau et al. 2011, [9] Combeau et al. 2012) are in generally good agreement, but differences can also be observed in quantitative comparisons, especially for the velocity at high liquid fraction. Therefore, more numerical comparisons of computer codes based on FEM and experimental results corresponding to the reference case are still needed to assess different numerical algorithms and more complex solidification models.

ACKNOWLEDGMENTS

This research was funded by the National Natural Science Foundation of China, grant number 51875307.

REFERENCES

1. Lesoult G 2005, 'Macrosegregation in steel strands and ingots: Characterisation, formation and consequences', *Materials Science and Engineering A*, vol. 413, no. 36, pp. 19-29.
2. Flemings MC & Nereo GE 1967, 'Macrosegregation: part I', *Transactions of the Metallurgical Society of AIME*, vol. 239, no. 9, pp. 1449-1461.
3. Ni J & Beckermann C 1991, 'A volume-averaged 2-phase model for transport phenomena during solidfication', *Metallurgical Transactions B-Process Metallurgy*, vol. 22, no. 3, pp. 349-361.
4. Bennon WD & Incropera FP 1987, 'A continuum model for momentum, heat and species transport in binary solid-liquid phase change systems. 1. Model formulation', *International Journal of Heat and Mass Transfer*, vol. 30, no. 10, pp. 2161-2170.
5. Li J, Wu M, Ludwig A, et al. 2012, 'Modelling macrosegregation in a 2.45 ton steel ingot', *2012 IOP Conference Series: Material Science and Engineering*, 33: 12091.
6. Bellet M, Combeau H, Fautrelle Y, et al. 2009, 'Call for contributions to a numerical benchmark problem for 2D columnar solidification of binary alloys', *International Journal of Thermal Sciences*, vol. 48, no. 11, pp. 2013-2016.
7. Choi HG, Choi H & Yoo JY 1997, 'A fractional four-step finite element formulation of the unsteady incompressible Navier-Stokes equations using SUPG and linear equal-order element methods', *Computer Methods in Applied Mechanics and Engineering*, vol. 143, no. 3-4, pp. 333-348.
8. Combeau H, Bellet M, Fautrelle Y, et al. 2011, 'A numerical benchmark on the prediction of macrosegregation in binary alloys', *TMS 2011 Annual Meeting Supplemental Proceedings: Materials Fabrication, Properties, Characterization, and Modeling*, Hoboken: John Wiley & Sons, Inc., pp. 755-762.
9. Combeau H, Bellet M, Fautrelle Y, et al. 2012, 'Analysis of a numerical benchmark for columnar solidification of binary alloys', *2012 IOP Conference Series: Materials Science and Engineering*, 33: 012086.
10. Carman PC 1937, 'Fluid flow through a granular bed', *Transactions Institute of Chemical Engineers*, vol.15, pp. 150-16.